*Journal of Statistical Physics, Vol. 100, Nos. 1/2, 2000*

# Computer Simulation of Irreversible Expansions *via* Molecular Dynamics, Smooth Particle Applied Mechanics, Eulerian, and Lagrangian Continuum Mechanics

**Wm. G. Hoover,[1] H. A. Posch,[2] V. M. Castillo,[3] and C. G. Hoover[3]**

*Received June 7, 1999; final September 3, 1999*

We simulate the far-from-equilibrium irreversible expansion of a compressed ideal gas in two space dimensions. For this problem the particle trajectories from conventional smooth particle applied mechanics are isomorphic to those from a corresponding molecular dynamics simulation. The smooth-particle "weight function" used to describe the expanding gas is identical to the pair potential governing the molecular dynamics simulation. These many-body particle simulations are compared with those using a modified smooth-particle algorithm invented by Monaghan, as well as with those based on conventional grid-based Eulerian and Lagrangian methods.

**KEY WORDS:** Irreversible expansion; smooth particles; Eulerian continuum mechanics; Lagrangian continuum mechanics.

## I. INTRODUCTION

Continuum flow problems can be solved by several "particle methods" as well as by using either fixed "Eulerian" or moving "Lagrangian" spatial grids. "Smooth-particle" methods can be used to derive ordinary differential motion equations for *particles* representing the *continuum* flow. The particle accelerations depend upon the *continuum* constitutive relations. Particle methods are specially easy to program. Smooth-particle methods also avoid

[1] Department of Applied Science, University of California at Davis/Livermore, and Lawrence Livermore National Laboratory, Livermore, California 94551-7808.
[2] Institut für Experimentalphysik, Universität Wien, A-1090 Vienna, Austria.
[3] Lawrence Livermore National Laboratory, Methods Development Group, Mechanical Engineering Department, Livermore, California 94551-7808.



0022-4715/00/0700-0313$18.00/0 

the "butterfly" and "hourglass" shear instabilities which can complicate Lagrangian grid-based solutions. The particle approaches are described in Section II. The grid-based approaches are described in Section III.

Our long-standing interest in simulating and understanding irreversible processes led us to study the irreversible confined expansion of a compressed ideal gas. An isoenergetic fourfold expansion should give an entropy increase of $k \ln 4$ per particle. As it does for *any* isolated Hamiltonian system, the incompressible form of Liouville's Theorem[1] implies that the statistical-mechanical Gibbs' entropy of the expanding fluid remains constant throughout the expansion process. Our detailed study[2] showed that a properly *coarse-grained* entropy actually increases very rapidly to the proper value—with most of the increase occuring within a single sound traversal time—even in the absence of any explicit transport coefficients in the deforming fluid. This rapid equilibration was surprising to us. To some extent it is an artifact of the relatively poor representation of interfaces and boundaries intrinsic to conventional particle methods. Two conventional smooth-particle fluids, colliding at sonic velocities, typically interpenetrate one another. But any reasonable boundary between two such colliding fluids would rule out such an unphysical interpenetration. Monaghan[3] has discussed these difficulties. He suggested and tested modified algorithms designed to avoid them, as is discussed in the following Section.

Numerical difficulties, associated with the propagation and collision of density discontinuities, led us to a smoother simpler version of the confined free expansion problem. We examined the equilibration of a periodic "sinusoidal" density profile using a simple "polytropic" (power law) equation of state, $P \propto \rho^2$. By using fixed viscosity and conductivity coefficients while increasing the system size we can systematically try to approach the wholly nondissipative Eulerian limit for this model. Our numerical results suggest that this problem is well-posed. It seems to us to be a useful test case for the evaluation and improvement of competing simulation methods. The sinusoidal equilibration problem is described in general terms in Section IV, and its solution is then approximated, through simulations using all four numerical methods, in the following Section V. Our conclusions make up the final Section VI.

## II. SPAM AND MOLECULAR DYNAMICS

Continuum mechanics treats the time-development of the mass density $\rho$, the velocity $v$, and the energy per unit mass $e$ throughout space. Conventional "SPAM" (Smooth Particle Applied Mechanics)[4–6] begins with the continuum *partial* differential equations linking the *time* development of the

density, velocity, and energy per unit mass to *spatial* derivatives. These partial differential equations are converted to a simpler finite set—we indicate such a set by using curly brackets $\{\cdots\}$—of *ordinary* differential equations for the *particle* variables—$\{r_i, v_i, e_i\}$. The resulting ordinary differential equations—five for each particle $i$: $1 \leqslant i \leqslant N$ in the two-dimensional case and seven in three dimensions—follow from the continuum constitutive equations. The *density* $\rho_i$ associated with each smooth particle is calculated by a direct summation over that particle's near neighbors:

$$\left\{\rho_i \equiv m \sum_j w(r_i - r_j)\right\}$$

Lucy's weight function is a typical choice for $w$. It is normalized, has a finite range $h$, and two continuous spatial derivatives:

$$w_{\text{Lucy}}(r < h) \equiv (5/\pi h^2)\left[1 + 3\frac{r}{h}\right]\left[1 - \frac{r}{h}\right]^3$$

$$\int_0^h 2\pi r w(r)\, dr \equiv 1$$

Thus the calculation of the particle densities $\{\rho_i\}$ reduces to evaluating simple sums and requires no time integration.

The smooth-particle equations of motion, giving the sets of particle coordinates and velocities, $\{r_i, v_i\}$, resemble Newton's motion equations for a corresponding set of molecular dynamical particles interacting with a pair potential $w(r)$:

$$\left\{\dot{r}_i = v_i;\ \dot{v}_i \equiv -m \sum_j \left[(P/\rho^2)_i + (P/\rho^2)_j\right] \cdot \nabla_i w(r_i - r_j)\right\}$$

Provided that the pressure tensor $P$ and mass density $\rho$ vary slowly, the particle accelerations $\{\dot{v}_i\}$ are proportional to pair sums of weight-function gradients. This interesting correspondence linking conventional SPAM to molecular dynamics can be made *exact*, with the SPAM weight function $w$ playing the role of a molecular dynamics pair potential. It is only necessary to adopt a simple polytropic equation of state for the equilibrium part of the pressure tensor: $P_{\text{eq}} \equiv \rho^2/2 \equiv \rho e$. We use this constitutive relation throughout, so that the conventional SPAM equations of motion are *identical* to that of conservative Newtonian molecular dynamics. We refer to these particle equations of motion, without any transport coefficients, as "SPAM" throughout the present work. For the ideal-gas polytropic equation of state the "energy equation" for the time development of the particle

energies $\{m_i \dot{e}_i\}$ is exactly equivalent to the particle version of the continuity equation for $\{\dot{\rho}_i\} \equiv 2m\{\dot{e}_i\}$. The usual transport coefficients—shear viscosity, bulk viscosity, and thermal conductivity—are all set equal to zero in this case. For simplicity in what follows we choose the particle mass $m$ equal to unity and the range of the weight function equal to six: $h = 6$, just as in ref. 2.

Although this conventional approach to continuum simulations, with the viscosities $(\eta, \eta_V)$ and heat conductivity $\kappa$ added, works perfectly well for *subsonic* flows like Rayleigh–Bénard convection, more *violent* flows lead to substantial unphysical interpenetration of opposing particle currents. To prevent this interpenetration, so as to preserve interfacial boundaries and to allow for the collision of solid bodies, Monaghan suggested a clever modification of SPAM,[3] in which the particle motions $\{v_i\}$ depend on a specially *averaged* velocity which differs little from the smooth-particle fluid velocity at each particle's location, $\langle v \rangle_i$:

$$\left\{ \dot{r}_i = v_i + m \sum_j (v_j - v_i)\, w_{ij}/\rho_{ij} \right\}$$

The symmetrized densities $\rho_{ij}$—either arithmetic or geometric means of the densities $\rho_i$ and $\rho_j$—are chosen to guarantee the conservation of (linear) momentum. The simpler approximation,

$$\left\{ \dot{r}_i = \langle v \rangle_i \equiv \sum_j (v_j)\, w_{ij} \Big/ \sum_j w_{ij} \right\}$$

is not conservative. Monaghan's modification of SPAM thus closely resembles ordinary Lagrangian continuum methods, but is immune to the tangling and shear instabilities which complicate those methods.

In addition to using an averaged velocity for moving particles, Monaghan included a repulsive central force, depending upon two parameters, $\alpha$ and $\beta$, while excluding conventional viscosity—guaranteeing the conservation of angular momentum as well as linear—between particles $i$ and $j$ whenever the two particles approach one another. Monaghan's extra force is closely analogous to von Neumann's "artificial viscosity," which was introduced to smooth out compressive velocity gradients. The parameters $\alpha$ and $\beta$ defined by Monaghan correspond to von Neumann's linear and quadratic artificial viscosities. In all of our implementations of Monaghan's ideas we have used the values which he recommended, $\alpha = 1$; $\beta = 2$. We will refer to Monaghan's modification of SPAM, with the symmetrized densities $\rho_{ij}$, as $\mathrm{SPAM_M}$.

## III. EULERIAN AND LAGRANGIAN CONTINUUM MECHANICS

The complete continuum equations for the time-development of the hydrodynamic density $\rho$, velocity $v$, and energy per unit mass $e$ include the pressure tensor $P$ and the heat flux vector $Q$. They can be expressed in either the fixed-grid Eulerian form:

$$\partial\rho/\partial t = -\nabla\cdot(\rho v)$$

$$\partial(\rho v)/\partial t = -\nabla\cdot(P+\rho vv)$$

$$\partial(\rho[e+\tfrac{1}{2}v^2])/\partial t = -\nabla\cdot(\rho v[e+\tfrac{1}{2}v^2]+v\cdot P+Q)$$

or the simpler comoving Lagrangian form:

$$\dot\rho/\rho = -\nabla\cdot v$$

$$\rho\dot v = -\nabla\cdot P$$

$$\rho\dot e = -\nabla v : P - \nabla\cdot Q$$

We will assume the usual Newtonian and Fourier versions of the transport coefficients, but with the special choice of bulk viscosity, $\eta_V \equiv (\eta/3)$. This *two*-dimensional constitutive equation corresponds to the *three*-dimensional choice $\eta_V = 0$.[7]

It is usual to evaluate all the necessary spatial derivatives in the continuum equations in terms of truncated centered-difference expressions, either at the grid points or at zone centers located between the points, converting all the partial differential equations for the evolution of the density, velocity, and energy into finite coupled sets of ordinary differential equations. Fixed-grid Eulerian simulations with the velocity and energy followed *at* the grid points and with density, stress, and heat flux followed at the *zone centers* can provide "useful" (inexpensive and stable) solutions to the Rayleigh–Bénard problem.[7–9] This same two-grid approach can be adapted to describe the equilibration of the highly nonlinear pressure waves described in what follows. Our preliminary investigations showed that the Eulerian simulations are *unstable* in the absence of dissipative transport coefficients. We accordingly have added three small constant transport coefficients to the centered-difference fixed-grid approximation to solving the continuum equations. The effect of these coefficients vanishes in the "continuum limit." This limit can be achieved in either of two equivalent ways: (i) by increasing the *number* of particles for a fixed system size, or (ii) by increasing the system *size* for fixed particle size and mass.

Moving-grid Lagrangian simulations, with *quadrilateral* zones in two dimensions, also require some viscosity for stability. Quadrilateral zones

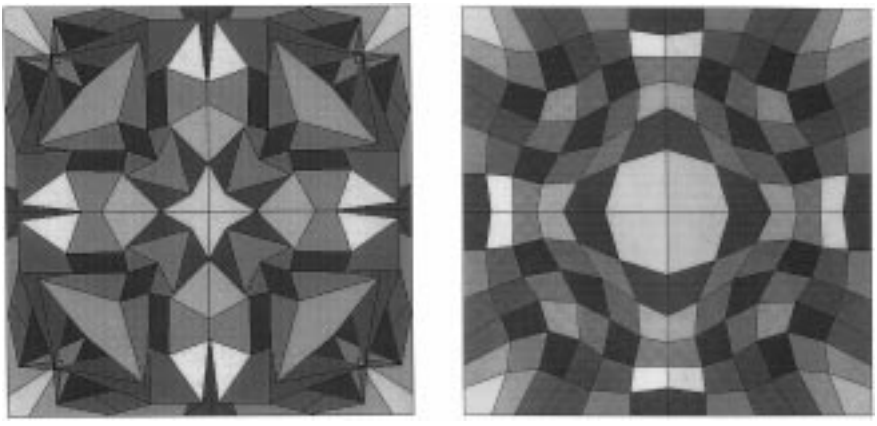

Fig. 1. Lagrangian $12 \times 12$ meshes after one "sound traversal time," $t = \tau$, both without (left) and with (right) butterfly–hourglass control. The sound traversal time is based on the (maximum) sound velocity, unity: $\tau \equiv L/c = L$. Both butterfly and hourglass instabilities can be seen within the lefthand mesh. The shading is used only to distinguish the zones from one another and has no special significance.

are chosen in order to facilitate shear deformation. As a result, *unstable* "butterfly" and "hourglass" modes, which can be seen in Fig. 1 (left), are common hazards to Lagrangian simulations. These modes correspond to a shear instability, with half of a zone undergoing *positive* shear and the other half *negative*, with no resulting overall restoring force. The two mode types—butterfly and hourglass—are linear combinations of one another for small strains. These unstable modes require damping too. When both the usual artificial viscosity and the additional butterfly–hourglass controls are included, the Lagrangian approach can likewise provide useful solutions.

## IV. IRREVERSIBLE EXPANSIONS

The confined free expansion which we studied previously[2] using conventional smooth-particle SPAM, showed very rapid equilibration. An expanding square of dense compressed ideal gas, confined to a larger periodic square container, appeared to be close to an equilibrium state after one or two sound traversal times. See Fig. 2. This qualitative visual evidence was confirmed by quantitative studies of the evolution of the kinetic and internal energies, as well as the entropy, for the expanding gas. These simulations appear to be rather unrealistic—the particles pass relatively freely *through* one another. Monaghan[3] had suggested a means to avoid this problem, as described in Section II. Our own attempts to solve this same periodic expansion problem with conventional Eulerian

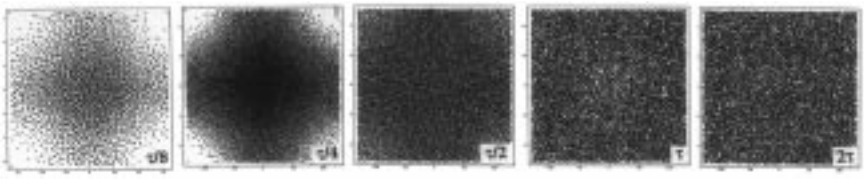

Fig. 2. Snapshots of a 16384-particle SPAM simulation of the equilibration of a *discontinuous* ideal-gas density distribution. The individual particle locations are shown at times, relative to the sound traversal time, of $t/\tau = \{1/8, 1/4, 1/2, 1, 2\}$. These data are from the detailed simulation described in ref. 2.

fixed-grid finite-difference techniques failed. We therefore sought out a different, but related, problem which would be accessible to all four schemes, both particle-based and grid-based. We found such a problem by eliminating the sharp discontinuities in the initial density profile.

All four numerical methods which we have considered are *consistent* with the continuum evolution equations and *stable* for sufficiently small perturbations from equilibrium. In order to compare the four techniques we have chosen to follow the motion of a highly-nonlinear, but periodic and continuous, density distribution, with the initial sinusoidal form:

$$\rho(x, y) \equiv f(x)\, f(y)$$

$$f(x) \equiv [\,1 + 0.9 \cos(kx)\,]/1.9$$

$$0.0526 \leqslant f \leqslant 1.0$$

where the constant $k$ is $(2\pi/L)$ and $L$ is the width of the periodic cell. The density varies by a factor of $19^2 = 361$: in the center of the periodically-repeated cell it takes on the maximum value of unity; the minimum density occurs at the cell vertices, 0.00277. In Fig. 3 (left) we show the initial Lagrangian mesh corresponding to this density distribution. Each of the zones shown contains the same mass. The initial condition for a smooth-particle simulation is also shown in that figure (right).

Figure 4 details the evolution of the sinusoidal initial condition according to the conventional SPAM algorithm. Just as before, the distribution of the particles becomes fairly homogeneous after two sound traversal times. In our earlier work[2] we focused our attention on the increase in the coarse-grained entropy density, $s(e_{\text{eff}}, \rho)$. We computed an effective internal energy per unit mass, $e_{\text{eff}}$, by using the smooth-particle weight functions to compute the thermal velocity fluctuations,

$$2e_{\text{eff}} \equiv \langle v^2 \rangle - \langle v \rangle^2$$

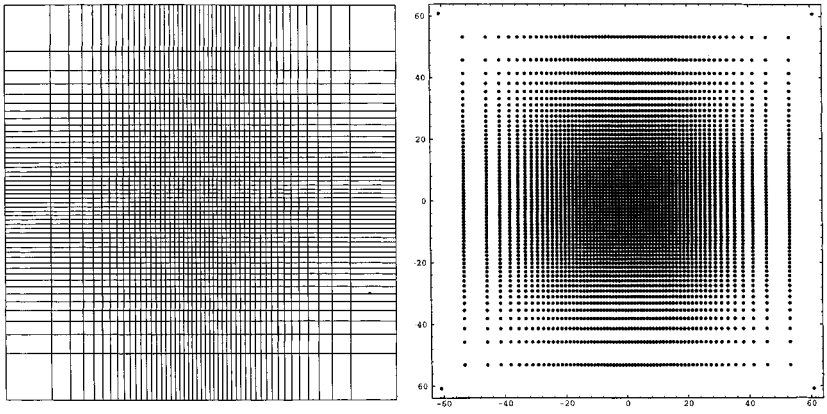


Fig. 3. The initial Lagrangian mesh for a $48 \times 48$ zone simulation (left). Each zone contains the same mass. The initial arrangement of $64 \times 64$ SPAM particles is shown too (right).

Because such velocity fluctuations are not present in the conventional Eulerian and Lagrangian methods which we use here, we have studied instead the time evolution of the *total* kinetic energy. It is to be expected that a part of the initial total internal energy,

$$E_0 = Nm\langle e \rangle_0 = \iint dx\, dy\, \tfrac{1}{2}\rho^2 \equiv (L^2/2)(1 + 0.405^2)/3.61^2$$

$$= (N/2)(1 + 0.405^2)/3.61 = 0.27341N$$

will generate a variety of sound waves through the nonlinear convective interactions. The ability to describe this process, over a period of several sound traversal times, is a relatively severe test of the various algorithms compared here. The Lyapunov instability of the SPAM algorithm and the artificial viscosities in the other methods prevent the exact reversibility of the evolutions.

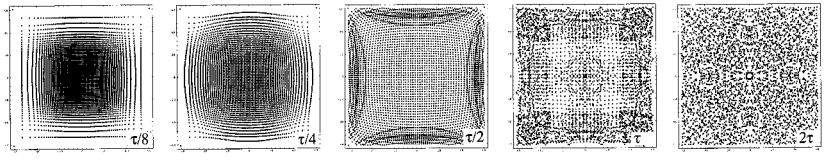


Fig. 4. Snapshots of a 4096-particle SPAM simulation of the equilibration of a *sinusoidal* ideal-gas density distribution. The individual particle locations are shown at times, relative to the sound traversal time, of $t/\tau = \{1/8, 1/4, 1/2, 1, 2\}$.

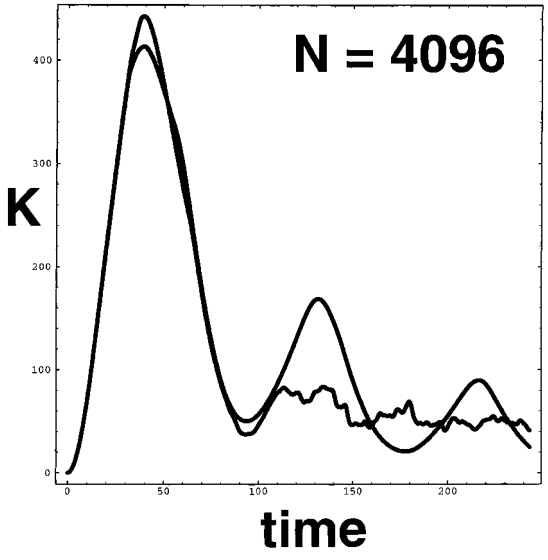


Fig. 5. Time history ($0 < t < 2\tau$) of the hydrodynamic (spatially-averaged) kinetic energy for 4096 particles. The ragged curve with the higher maximum corresponds to the conventional SPAM algorithm. The smooth curve corresponds to Monaghan's modification $\mathrm{SPAM}_{\mathrm{M}}$.

## V. RESULTS

It soon became apparent that conventional SPAM blurs the hydrodynamic flow field as the expanding parts of the flow penetrate into the lower-density regions. The corresponding time history of the total hydrodynamic kinetic energy, $\sum_j \frac{1}{2}(\langle \rho \rangle_j \langle v \rangle_j^2)$, when fluctuations are excluded, is the relatively ragged curve shown in Fig. 5. In the same figure we display the corresponding kinetic energy using Monaghan's modified algorithm, discussed below.

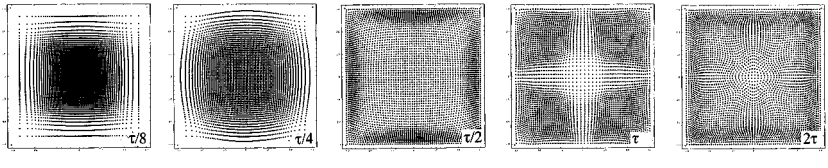


Fig. 6. Snapshots of a 4096-particle $\mathrm{SPAM}_{\mathrm{M}}$ simulation of the equilibration of a *sinusoidal* ideal-gas density distribution. The individual particle locations are shown at times, relative to the sound traversal time, of $t/\tau = \{1/8, 1/4, 1/2, 1, 2\}$.

The trouble with the conventional smooth-particle method is that the *boundary* conditions are not implemented well. Particles pass through each other. Monaghan suggested not only using an artificial viscosity, but also the modified equations of motion discussed at the end of Section II. We have implemented his idea, and the effect can be seen by comparing the two kinetic energies shown in Fig. 5. Note that the "ringing" of the kinetic energy is much more peristent with the improved $\text{SPAM}_{\text{M}}$ algorithm. The smooth-particle trajectories in Fig. 6 show that there is *no* interpenetration

**Table I. Per-particle Kinetic Energy Maxima and Minima for the Four Simulation Techniques Described in the Text (Euler, Lagrange, SPAM, Monaghan)[a]**

| Type | $N$ or $V$ | $t_{\max}$ | $K_{\max}$ | $t_{\min}$ | $K_{\min}$ |
|---|---|---|---|---|---|
| Euler(0.05) | $V=12^2$ | 4.0 | 2.98 | 9.5 | 0.16 |
| Euler(0.05) | $V=24^2$ | 8.0 | 14.40 | 18.9 | 1.58 |
| Euler(0.05) | $V=48^2$ | 16.1 | 63.60 | 38.3 | 9.46 |
| Euler(0.05) | $V=96^2$ | 32.3 | 269.38 | 77.3 | 44.22 |
| Euler(0.05) | $V=192^2$ | 64.9 | 1113.66 | 155.0 | 190.08 |
| Euler(0.10) | $V=12^2$ | 3.7 | 2.26 | 9.5 | 0.02 |
| Euler(0.10) | $V=24^2$ | 7.7 | 12.18 | 18.6 | 0.56 |
| Euler(0.10) | $V=48^2$ | 15.8 | 57.64 | 37.8 | 5.82 |
| Euler(0.10) | $V=96^2$ | 32.1 | 254.40 | 77.0 | 34.64 |
| Euler(0.10) | $V=192^2$ | 64.7 | 1077.52 | 155.5 | 162.00 |
| Lagrange | $V=12^2$ | 2.7 | 4.13 | 8.0 | 0.38 |
| Lagrange | $V=24^2$ | 5.5 | 17.31 | 16.0 | 2.27 |
| Lagrange | $V=48^2$ | 11.8 | 70.71 | 32.3 | 11.15 |
| Lagrange | $V=96^2$ | 23.7 | 285.17 | 65.2 | 49.86 |
| Lagrange | $V=192^2$ | 48.0 | 1145.32 | 130.0 | 216.10 |
| SPAM | $N=32^2$ | 19.9 | 104.78 | 47.7 | 6.38 |
| SPAM | $N=64^2$ | 39.1 | 442.60 | 93.2 | 37.22 |
| SPAM | $N=128^2$ | 79.0 | 1800.22 | 195.2 | 175.98 |
| SPAM | $N=256^2$ | 158.8 | 7011.51 | 392.7 | 727.49 |
| $\text{SPAM}_{\text{M}}$ | $N=32^2$ | 17.9 | 94.27 | 45.7 | 7.47 |
| $\text{SPAM}_{\text{M}}$ | $N=64^2$ | 39.2 | 413.22 | 93.6 | 50.27 |
| $\text{SPAM}_{\text{M}}$ | $N=128^2$ | 79.8 | 1742.64 | 191.3 | 250.63 |
| $\text{SPAM}_{\text{M}}$ | $N=256^2$ | 161.6 | 7164.72 | 388.3 | 1112.99 |

[a] The number of particles $N$ or the volume $V \equiv 3.61N$, and the time and size of the first kinetic-energy maximum and minimum are given. The Eulerian transport coefficients ($\eta = \kappa = 3\eta_V$) are given in parentheses. The Lagrangian viscosities and controls all take on their conventional default values.

with this algorithm. Compare Figs. 4 and 6. We carried out a few additional simulations replacing Monaghan's "new" particle motion equations,

$$\left\{\dot{r}_i = v_i + m \sum_j (v_j - v_i)\, w_{ij}/\rho_{ij}\right\}$$

with the simpler ones used in conventional Lagrangian simulations:

$$\{\dot{r}_i \equiv \langle v \rangle_{(r_i)}\}$$

but retaining his linear and quadratic artificial viscosities. The changed equations of motion made no significant difference to the evolution.

Eulerian equilibration simulations required a small nonvanishing viscosity for stability, as explained in Section III. Once this was included, the resulting kinetic energy histories approach the large-system (or small-mesh) continuum limit, with deviations of order $1/L$. This dependence is quite apparent from the data given in Table I. The linear extrapolations to

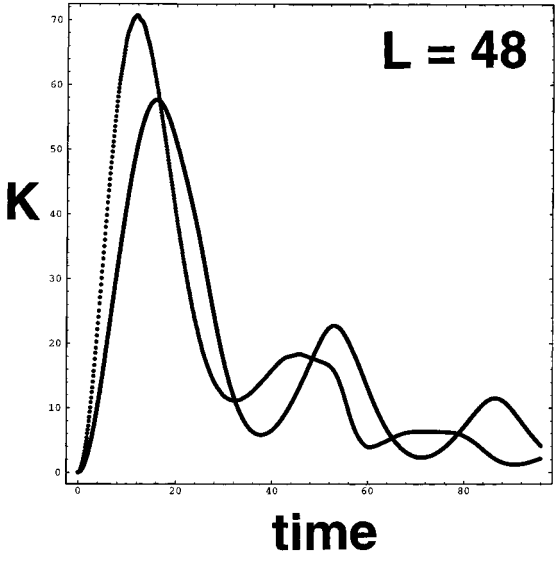


Fig. 7. Time histories of the kinetic energy $K$ with $L = 48$ according to conventional Eulerian and Lagrangian continuum simulations with $0 < t < 2\tau = 96$. The Lagrangian curve has the higher maximum. The Eulerian simulation incorporates a shear viscosity coefficient of 0.10.

$L \to \infty$ (or to zero mesh size with $L$ fixed) all agree within statistical errors, suggesting that this problem is well posed. The agreement with the Lagrangian and $\mathrm{SPAM}_{\mathrm{M}}$ extrapolations also suggests, with the exception of the conventional SPAM algorithm, that the numerical approaches *all* converge to the *same* solution as the resolution is improved. The Eulerian and Lagrangian kinetic energy histories both appear in Fig. 7. Density surfaces at times corresponding to the first maximum and minimum in the kinetic energy appear in Fig. 8.

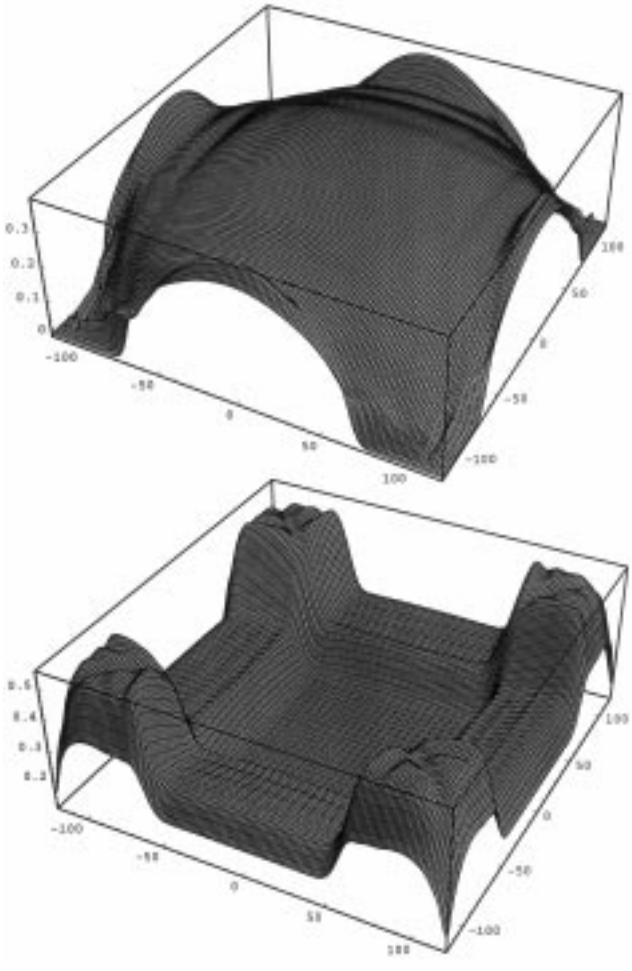


Fig. 8. Density surfaces at times corresponding to the first kinetic-energy maximum (left) and minimum (right) according to the $\mathrm{SPAM}_{\mathrm{M}}$ algorithm.

## VI. CONCLUSIONS

Among the four techniques compared here, the smooth-particle algorithm, Monaghan's modification of it, and the Eulerian algorithm, are all relatively easy to program. $SPAM_M$, with Monaghan's special motion equations and artificial viscosity included, does a very nice job of handling the complex wave interactions generated by nonlinear convection. The Lagrangian simulation, on the other hand, requires a significant programming effort, and is accordingly somewhat more difficult to optimize. Despite the three different Lagrangian viscosities used, with the recommended values in each case, highly-compressed zones near the corners exhibit unacceptable distortions. Because the pressure is quadratic in the density, the resulting negative zone volumes do not lead to fatal instabilities. The Eulerian technique, though well-suited to this symmetric problem, would have difficulty treating more-complex flows. With the exception of the conventional SPAM algorithm (with *vanishing* transport coefficients), *all* the numerical methods just mentioned can be used to solve this interesting problem. Among the various methods the Lagrangian technique shows the least number dependence—and is thus the best technique for this problem—but at the cost of increased complexity in the programming.

## ACKNOWLEDGMENTS

The present work began at the University of Vienna during an Erwin Schrödinger Institute workshop. Work at the Lawrence Livermore National Laboratory was performed under the auspices of the United States Department of Energy under University of California Contract W-7405-Eng-48. We thank Peter Raboin and Jerry Lin for their support of this work at Livermore. The work was additionally supported by a grant to HAP from the Fonds zur Förderung der wissenschaftlichen Forschung, Grant P11428-PHY.

## REFERENCES

1. Wm. G. Hoover, Liouville's theorems, Gibbs' entropy, and multifractal distributions for nonequilibrium steady states, *J. Chem. Phys.* **109**:4164–4170 (1998).
2. Wm. G. Hoover and H. A. Posch, Entropy increase in confined free expansions *via* molecular dynamics and smooth-particle applied mechanics, *Phys. Rev. E* **59**:1770–1776 (1999).
3. J. J. Monaghan, On the problem of penetration in particle methods, *J. Comput. Phys.* **82**:1–15 (1989).
4. L. Lucy, A numerical approach to the testing of the fission hypothesis, *Astron. J.* **82**:1013–1024 (1977).

5. J. J. Monaghan, Smoothed particle hydrodynamics, *Ann. Rev. Astron. Astrophys.* **30**:543–574 (1992).
6. Wm. G. Hoover, C. G. Hoover, O. Kum, V. M. Castillo, H. A. Posch, and S. Hess, Smooth particle applied mechanics, *Computational Methods in Science and Technology* **2**:65–72 (1996).
7. V. M. Castillo, Wm. G. Hoover, and C. G. Hoover, Coexisting attractors in compressible Rayleigh–Bénard flow, *Phys. Rev. E* **55**:5546–5550 (1997).
8. M. Mareschal and E. Kestmont, Experimental evidence for convective rolls in finite two-dimensional molecular models, *Nature* **329**:427–428 (1987).
9. O. Kum, Wm. G. Hoover, and H. A. Posch, Viscous conducting flows with smooth-particle applied mechanics, *Phys. Rev. E* **52**:4899–4908 (1995).